

Quasifree electrofission of ^{238}U

V. P. Likhachev,¹ J. Mesa,^{1,2} J. D. T. Arruda-Neto,^{1,3} B. V. Carlson,⁴ A. Deppman,¹ M. S. Hussein,¹ V. O. Nesterenko,⁵ F. Garcia,⁶ and O. Rodriguez²

¹*Instituto de Física, Universidade de São Paulo, São Paulo, Brazil*

²*Instituto Superior de Ciencias y Tecnologia Nucleares, Havana, Cuba*

³*Universidade de Santo Amaro, São Paulo, Brazil*

⁴*Instituto de Estudos Avançados-Centro Técnico Aeroespacial, São José dos Campos, Brazil*

⁵*Bogoliubov Laboratory of Theoretical Physics, JINR, Dubna, Russia*

⁶*Universidade Estadual de Santa Cruz, Ilheus, Bahia, Brazil*

(Received 21 September 2001; published 27 March 2002)

We present the result of a theoretical study of the quasifree electrofission of ^{238}U . The exclusive differential cross sections for the quasifree scattering reaction stage have been calculated in plane wave impulse approximation, using a macroscopic-microscopic approach for the description of the proton bound states. The nuclear shape was parametrized in terms of Cassinian ovoids. The equilibrium deformation parameters have been calculated by minimizing the total nuclear energy. In the calculation the axially deformed Woods-Saxon single-particle potential was used. The obtained single-particle momentum distributions were averaged over the nuclear symmetry axis direction. The occupation numbers were calculated in the BCS approach. The fissility for the single-hole excited states of the residual nucleus ^{237}Pa was calculated on the statistical theory grounds, both without taking into account the preequilibrium emission of the particle and with preequilibrium emission in the framework of the exciton model.

DOI: 10.1103/PhysRevC.65.044611

PACS number(s): 24.60.Dr, 24.75.+i, 21.60.Ev, 27.90.+b

I. INTRODUCTION

Quasifree (QF) scattering of high energy electrons on nuclei is the field of nuclear physics which is traditionally devoted to the study of the single-particle aspects of nuclear structure: single-particle binding energies, momentum distributions, occupation numbers, etc. [1].

A new branch of these investigations is the study of decay channels of single-hole states in the residual nucleus, created as a result of the QF process. Especially interesting is to study a fission decay following a QF process. In this case we have a single-particle process in the first reaction stage, and essentially a collective process in the final reaction stage. The collective degrees of freedom are excited in the intermediate reaction stage due the residual interaction.

This is a new sort of nuclear reaction, which may allow one to get unique information on the dissociation of well defined single-hole configurations [which we can select by coincidence $(e, e'p)$] into complex nuclear configurations, and its role in nuclear fission. The new and most important aspect of this reaction is that, after knocking out a proton, we obtain the heavy nucleus ^{237}Pa in a single-hole doorway state (see discussion below), which could undergo nuclear fission. Indeed, instead of dealing with collective doorway states, which are coherent sums of a great number of $1p-1h$ configurations (as the well-known giant resonances), these non-collective doorway states will be represented by only one, well defined, $1h$ configuration. The residual interaction in ^{237}Pa mixes these $1h$ configurations into more complicate $2h-1p$ and $3h-2p$ ones. So, there would be some competing channels for fission. It may occur either directly from $1h$ configurations, or, with some delay, from mixed states (or their components). In a QF process we have in the initial state only one configuration; thus, the fission probability P_f

should be more sensitive to the individual structure of this initial state as compared with conventional reactions, where the effects of the structure are averaged out over many single-particle states forming the doorway.

The unambiguous extraction of single-hole contributions is possible only in an exclusive experimental scheme [reaction $(e, e'pf)$] and involves extremely thin targets (fission fragments have to leave the target with small energy losses), high energy resolution, and coincidence requirement between the final particles in order to separate the single-hole states. The exclusive $(e, e'pf)$ experiment is very difficult for practical realization, and has never been performed so far. The integral contribution of the quasifree electron scattering to the fission process was studied only in inclusive experiments: (e, f) [2] and $(e, e'f)$ [3]. These works dealt only with the issue of the QF contribution in electrofission.

The advent of high energy, cw, electron accelerators combined with the development of high resolution facilities, opens the possibility of studying the fission channel for quasifree electron scattering in an exclusive experimental setup. The most suitable accelerator for this experiment is at the Thomas Jefferson National Accelerator Facility (TJNAF).

For excitation of the residual nucleus to a well-defined single-hole state, the initial and final state interactions have to be negligible. This situation corresponds to high momentum transfer and high proton exit energy, when the plane wave impulse approximation (PWIA) for the calculation of the quasifree electron scattering cross section is valid.

This work presents the results of PWIA calculations for the quasifree $(e, e'p)$ -differential cross section for deformed orbitals of ^{238}U , in the framework of the macroscopic-microscopic approach, plus an estimate of the fissility for single-hole states in the residual nucleus ^{237}Pa , performed on the statistical theory grounds. These calculations could serve

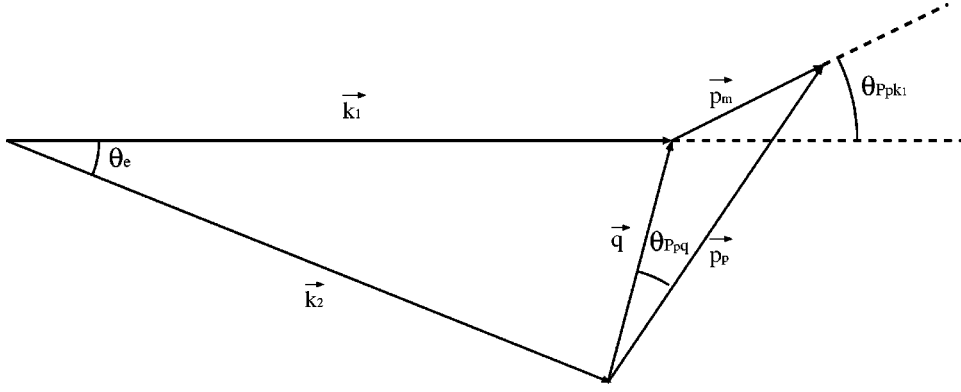


FIG. 1. Momentum diagram of the $A(e, e'p)A-1$ reaction in the impulse approximation: \vec{k}_1 and \vec{k}_2 are the initial and final electron momenta, respectively; \vec{p}_m is the momentum of proton before interaction; \vec{p}_p is the momentum of knocked-out proton.

as first order magnitude guideline for expected cross sections.

II. PWIA CROSS SECTION

In the first order Born approximation the electron with initial four-momentum $k_{1\mu} = (\vec{k}_1, i\varepsilon_1)$ and final $k_{2\mu} = (\vec{k}_2, i\varepsilon_2)$ transfers a virtual photon with four-momentum $q_\mu = (\vec{q}, i\omega) = k_{1\mu} - k_{2\mu}$, resulting in the final state a knocked-out nucleon with $p_\mu = (\vec{p}_p, iE_p)$ and a residual nucleus with $P_{A-1\mu} = (\vec{P}_{A-1}, iE_{A-1})$.

In the impulse approximation a virtual photon interacts with a bound nucleon (proton or neutron) of four-momentum $p_m = (\vec{p}_m, iE_m)$, which exits the nucleus with four-momentum $p_\mu = (\vec{p}_p, iE_p)$ without further interaction (no final state interaction). The corresponding momentum diagram in the impulse approximation is shown in Fig. 1 for the laboratory system.

In the PWIA $\vec{p}_m = -\vec{P}_{A-1}$, and the missing quantities (momentum and energy of the proton before interaction) can be defined from the energy and momentum conservation law in the following way:

$$\begin{aligned} \vec{p}_m &= \vec{p}_p - \vec{q}, \\ E_m &= \omega - T_p - T_{A-1}, \end{aligned} \quad (1)$$

where $E_m = M_{A-1} + m_p - M_A$ is the proton missing (or separation) energy, T_p is the kinetic energy of the outgoing proton, and T_{A-1} is the kinetic energy of the residual nucleus. The momentum and energy transfer of the virtual photon can be varied independently.

In the PWIA the sixfolded differential cross section of the $(e, e'p)$ reaction in the laboratory system has the following form [4]:

$$\frac{d^6\sigma}{d\Omega_e d\Omega_p d\varepsilon_2 dE_p} = p_p E_p \sigma_{ep} S(E_m, \vec{p}_m), \quad (2)$$

where

$$\sigma_{ep} = \sigma_{mott} (V_C W_C + V_T W_T + V_I W_I + V_S W_S) \quad (3)$$

is the off-shell electron-nucleon cross section and $S(E_m, \vec{p}_m)$ is the spectral function that defines the combined probability to find a bound proton with momentum \vec{p}_m on the shell with separation energy E_m .

The kinematic functions V in Eq. (3) can be expressed, neglecting the mass of the electron, as

$$V_C = \frac{q_\mu^4}{q^4}, \quad (4)$$

$$V_T = \frac{q_\mu^2}{2q^2} + \tan^2\left(\frac{\theta_e}{2}\right), \quad (5)$$

$$V_I = \frac{q_\mu^2}{q^2} \cos\phi \sqrt{\frac{q_\mu^2}{q^2} + \tan^2\left(\frac{\theta_e}{2}\right)}, \quad (6)$$

$$V_S = \frac{q_\mu^2}{q^2} \cos^2\phi + \tan^2\left(\frac{\theta_e}{2}\right), \quad (7)$$

and

$$\sigma_{mott} = \frac{\alpha^2 \cos^2\frac{\theta_e}{2}}{4\varepsilon_1^2 \sin^4\frac{\theta_e}{2}} \left(1 + \frac{2\varepsilon_1}{m_p} \sin^2\frac{\theta_e}{2}\right)^{-1} \quad (8)$$

is the Mott cross section, ϕ is the angle between the scattering plane and the plane defined by the vectors \vec{p}_p and \vec{q} .

For the structure functions W in Eq. (3) we use the off-shell prescription of de Forest [4]

$$W_C = \frac{1}{4\bar{E}E_p} \left\{ (\bar{E} + E_p)^2 \left(F_1^2 + \frac{\bar{q}_\mu^2}{4m_p^2} \kappa_p^2 F_2^2 \right) - q^2 (F_1 + \kappa_p F_2)^2 \right\},$$

$$W_T = \frac{\bar{q}_\mu^2}{2\bar{E}E_p} (F_1 + \kappa_p F_2)^2,$$

$$W_I = -\frac{p_p \sin \gamma}{\bar{E} E_p} (\bar{E} + E_p) \left(F_1^2 + \frac{\bar{q}_\mu^2}{4m_p^2} \kappa_p^2 F_2^2 \right),$$

$$W_S = \frac{p_p^2 \sin^2 \gamma}{\bar{E} E_p} \left(F_1^2 + \frac{\bar{q}_\mu^2}{4m_p^2} \kappa_p^2 F_2^2 \right), \quad (9)$$

where $\kappa_p = 1.793$ is the anomalous magnetic moment of the proton in units of the Bohr magneton

$$\bar{E} = \sqrt{p_m^2 + m_p^2}, \quad (10)$$

m_p is the mass of the proton, $\vec{q}_\mu = (\vec{q}, i\bar{\omega})$, $\bar{\omega} = E_p - \bar{E}$, γ is the angle between \vec{p}_p and \vec{q} . F_1 and F_2 are the on-shell Dirac and Pauli proton form factors, respectively,

$$F_1(q_\mu^2) = \frac{1}{1 + \frac{q_\mu^2}{4m_p^2}} \left[G_E(q_\mu^2) + \frac{q_\mu^2}{4m_p^2} G_M(q_\mu^2) \right], \quad (11)$$

$$\kappa_p F_2(q_\mu^2) = \frac{1}{1 + \frac{q_\mu^2}{4m_p^2}} [G_M(q_\mu^2) - G_E(q_\mu^2)], \quad (12)$$

where

$$G_E(q_\mu^2) = \left(\frac{1}{1 + \frac{q_\mu^2}{0.71}} \right)^{-2}, \quad (13)$$

$$G_M(q_\mu^2) = \mu_p G_E(q_\mu^2), \quad (14)$$

$\mu_p = 2.793$ is the proton magnetic moment in units of the Bohr magneton and q_μ^2 in Eq. (13) is in $(\text{GeV}/c)^2$.

In the independent particle shell model the spectral function for the spherical orbitals $\alpha \equiv n l j$ with binding energy E_α takes the simple form

$$S(E_m, \vec{p}_m) = \delta(E - E_\alpha) v_\alpha^2 n_\alpha(\vec{p}_m), \quad (15)$$

where v_α^2 and $n_\alpha(\vec{p}_m)$ are the occupation number and momentum distribution of the α orbital, respectively. The sixfolded ($e, e' p$) cross section could be transformed into a fivefolded one as

$$\frac{d^5 \sigma}{d\Omega_e d\Omega_p dE_p} = p_p E_p \sigma_{ep} v_\alpha^2 n_\alpha(\vec{p}_m), \quad (16)$$

where it is imposed energy and momentum conservation for the kinematics variables in σ_{ep} .

III. SINGLE-PARTICLE BOUND STATES

The single-particle bound state energies and momentum distributions were calculated in the framework of the macroscopic-microscopic approach by using the BARRIER code [5].

The energy of the nucleus is presented as

$$E_{tot} = E_{LD} + \delta E_{shell}, \quad (17)$$

where E_{LD} is the macroscopic liquid drop part of the energy and δE_{shell} is the shell correction, which describes shell and pairing effects. Both shell correction and the macroscopic part of the energy have been calculated according to [5].

A. Nuclear shape parametrization

Only axially symmetric nuclear shapes have been considered in the present work, and the deformed shape (up to and beyond its separation into two fragments) can be conveniently described by the Cassini ovoids [6,7]. The potential-energy surfaces are calculated as functions of ε (elongation) and α_4 (hexadecapolar momentum). From these potential-energy surfaces, the equilibrium (ground state) deformation parameters ε and α_4 were calculated by minimizing the total nuclear energy [Eq. (17)], $\varepsilon = 0.227$ and $\alpha_4 = 0.059$.

B. Nuclear potential

A Woods-Saxon potential [8], consisting of the central part V , spin-orbit V_{so} , and the Coulomb potential V_{Coul} for protons, was employed as

$$V^{WS}(r, z, \varepsilon, \hat{\alpha}) = V(r, z, \varepsilon, \hat{\alpha}) + V_{so}(r, z, \varepsilon, \hat{\alpha}) + V_{Coul}(r, z, \varepsilon, \hat{\alpha}). \quad (18)$$

The real potential $V(r, z, \varepsilon, \hat{\alpha})$ involves the parameters V_0 , r_0 , and a , describing the depth of the central potential, the radius, and the diffuseness parameter, respectively, and it is expressed as

$$V(r, z, \varepsilon, \hat{\alpha}) = \frac{V_0}{1 + \exp\left[\frac{Dist(r, z, \varepsilon, \hat{\alpha})}{a}\right]}, \quad (19)$$

where $Dist(r, z, \varepsilon, \hat{\alpha})$ is the distance between a point and the nuclear surface, and ε and $\hat{\alpha}$ are deformation parameters.

The depth of the central potential is parametrized as

$$V_0 = V_0 [1 \pm \kappa(N - Z)/(N + Z)] \quad (20)$$

with the plus sign for protons and the minus sign for neutrons, with the constant $\kappa = 0.63$.

The spin-orbit interaction is then given by

$$V_{so}(r, z, \varepsilon, \hat{\alpha}) = \lambda \left(\frac{\hbar}{2Mc} \right)^2 \nabla V(r, z, \varepsilon, \hat{\alpha}) \cdot (\vec{\sigma} \times \vec{p}), \quad (21)$$

where λ denotes the strength of the spin-orbit potential and M is the nucleon mass. The vector operator $\vec{\sigma}$ stands for Pauli matrices and \vec{p} is the linear momentum operator.

The Coulomb potential is assumed to be that corresponding to the nuclear charge $(Z - 1)e$, taken to be uniformly distributed inside the nucleus. It is computed in cylindrical coordinates by using the expression given in [6].

C. Single-particle potential parameter definitions

For the ground state deformation of ^{238}U , small changes in λ (spin-orbit potential strength) and $r_{0-s.o}$ (spin-orbit potential radius) of the Chepurnov parameters [9] are introduced in order to reproduce adequately the spin/parity of the levels sequence. Using single-particle states obtained by this procedure, the quasiparticle states can be calculated for the first minimum region, providing spin, parity, energy, and level spacing for the ground and some low-lying states. The quasiparticle spectrum was obtained by using the semimicroscopic combined method [10].

The potential parameters were chosen to give the best fit to the spectrum of single-quasiparticle excitations of the Z-odd neighboring nuclei ^{239}Np .

D. Single-particle wave functions

The Hamiltonian matrix elements are calculated with the wave functions of a deformed axially symmetric oscillator potential. The wave functions in the coordinate space ϕ_i are expanded into eigenfunctions of the axially deformed harmonic oscillator potential.

These eigenfunctions form a complete orthonormal basis for the single-particle Woods-Saxon wave function

$$\Psi_i(\vec{R}, \sigma) = \sum_{n_\rho, n_z, \Lambda, \Sigma} C_{n_\rho, n_z, \Lambda, \Sigma}^i \Phi_{n_\rho, n_z, \Lambda, \Sigma}(\vec{R}, \sigma). \quad (22)$$

From this expansion, we may conveniently express the single-particle Woods-Saxon wave function in momentum space

$$\overline{\Psi}_i(\vec{K}, \sigma) = \sum_{n_\rho, n_z, \Lambda, \Sigma} C_{n_\rho, n_z, \Lambda, \Sigma}^i \overline{\Phi}_{n_\rho, n_z, \Lambda, \Sigma}(\vec{K}, \sigma) \quad (23)$$

with

$$\overline{\Phi}_{n_\rho, n_z, \Lambda, \Sigma}(\vec{K}, \sigma) = \frac{1}{2\pi^{3/2}} \int d\vec{R} e^{-i\vec{K}\cdot\vec{R}} \Phi_{n_\rho, n_z, \Lambda, \Sigma}(\vec{R}, \sigma) \quad (24)$$

normalized to one.

We define densities $n_i(\vec{K})$ in momentum space in an analogous way to that in the configuration space,

$$\rho_i(\vec{R}) = \rho_i(r, z) = |\Phi_i^+(r, z)|^2 + |\Phi_i^-(r, z)|^2, \quad (25)$$

with

$$\begin{aligned} \Phi_i^\pm(r, z) &= \frac{1}{\sqrt{2\pi}} \sum_{n_\rho, n_z, \Lambda, \Sigma} \delta_{\Sigma, \pm 1/2} \delta_{\Lambda, \pm \Lambda} C_{n_\rho, n_z, \Lambda, \Sigma}^i \\ &\quad \times \Phi_{n_\rho, n_z, \Lambda, \Sigma}(\vec{R}, \sigma), \end{aligned} \quad (26)$$

and

$$n_i(\vec{K}) = n_i(k, k_z) = |\overline{\Phi}_i^+(k, k_z)|^2 + |\overline{\Phi}_i^-(k, k_z)|^2, \quad (27)$$

with

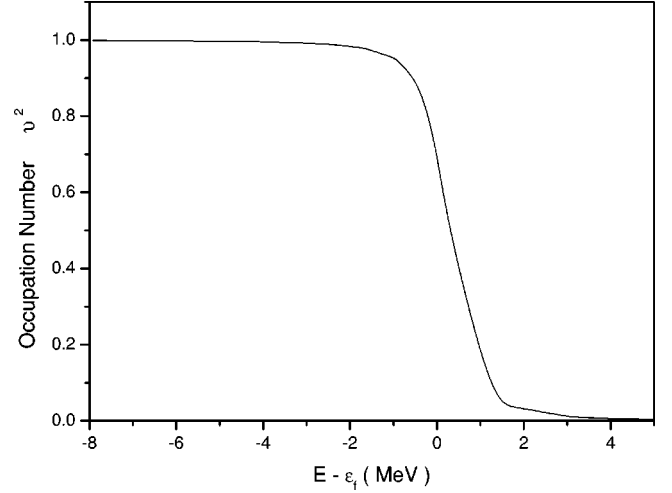


FIG. 2. Occupation probabilities for the single-particle bound states of ^{238}U .

$$\begin{aligned} \overline{\Phi}_i^\pm(k, k_z) &= \frac{1}{\sqrt{2\pi}} \sum_{n_\rho, n_z, \Lambda, \Sigma} \delta_{\Sigma, \pm 1/2} \delta_{\Lambda, \pm \Lambda} \\ &\quad \times C_{n_\rho, n_z, \Lambda, \Sigma}^i \overline{\Phi}_{n_\rho, n_z, \Lambda, \Sigma}(\vec{K}, \sigma). \end{aligned} \quad (28)$$

These single-particle momentum distributions $n_i(\vec{K})$ were averaged over nuclear symmetry axis directions.

Similar to the total density

$$\rho(\vec{R}) = \sum_i 2v_i^2 \rho_i(\vec{R}), \quad (29)$$

the total momentum distribution is given by

$$n(\vec{K}) = \sum_i 2v_i^2 n_i(\vec{K}), \quad (30)$$

where v_i^2 is the occupation probability resulting from the BCS model [10,11].

The results for the occupation number calculations are shown in Fig. 2. The energies of the ^{238}U proton bound states are shown in Table I.

IV. FISSILITY

The quasifree knockout of nucleons leads to the excitation of the residual nucleus. This excitation energy (E^* , nucleus $A-1$) has two origins: holes in the shells of the nucleus A , which appear as a result of the knockout of nucleons, and final state interaction (FSI) of the outgoing nucleon, which we assume as negligible due to the high energy of the proton.

The fast, quasifree reaction stage occurs at zero thermal excitation (ground state) of the initial nucleus ^{238}U , and results in a single hole in one of the shells. This single-hole configuration forms a doorway for a thermalization process that leads to the thermal excitation E^* of the residual nucleus ^{237}Pa .

The thermalization is a complicate process that involves

TABLE I. Proton single-particle levels of ^{238}U . The Fermi level is the level 46.

	(MeV)	πJ	$[Nn_z\Lambda]$		(MeV)	πJ	$[Nn_z\Lambda]$		(MeV)	πJ	$[Nn_z\Lambda]$
1	-33.685	1/2	1/2 [0 0 0]	23	-16.192	-3/2	3/2 [3 0 1]	45	-7.491	3/2	3/2 [4 0 2]
2	-31.397	-1/2	1/2 [1 1 0]	24	-15.490	-1/2	1/2 [3 0 1]	46	-7.195	1/2	1/2 [4 0 0]
3	-30.043	-3/2	3/2 [1 0 1]	25	-15.415	7/2	7/2 [4 1 3]	47	-6.277	5/2	5/2 [6 4 2]
4	-29.670	-1/2	1/2 [1 0 1]	26	-14.529	9/2	9/2 [4 0 4]	48	-6.189	-5/2	5/2 [5 2 3]
5	-28.141	1/2	1/2 [2 2 0]	27	-14.302	3/2	3/2 [4 2 2]	49	-5.348	-3/2	3/2 [5 2 1]
6	-26.630	3/2	3/2 [2 1 1]	28	-13.984	-1/2	1/2 [5 3 0]	50	-4.827	7/2	7/2 [6 3 3]
7	-25.963	1/2	1/2 [2 1 1]	29	-13.111	1/2	1/2 [4 2 0]	51	-4.340	-7/2	7/2 [5 1 4]
8	-25.542	5/2	5/2 [2 0 2]	30	-13.091	-3/2	3/2 [5 4 1]	52	-3.949	-1/2	1/2 [5 2 1]
9	-24.473	3/2	3/2 [2 0 2]	31	-12.383	5/2	5/2 [4 1 3]	53	-3.667	1/2	1/2 [6 5 1]
10	-24.025	-1/2	1/2 [3 3 0]	32	-11.735	-5/2	5/2 [5 3 2]	54	-3.465	-5/2	5/2 [5 1 2]
11	-22.836	1/2	1/2 [2 0 0]	33	-11.053	7/2	7/2 [4 0 4]	55	-3.417	9/2	9/2 [6 2 4]
12	-22.716	-3/2	3/2 [3 2 1]	34	-10.831	3/2	3/2 [4 1 1]	56	-3.051	-9/2	9/2 [5 0 5]
13	-21.614	-1/2	1/2 [3 2 1]	35	-10.388	-1/2	1/2 [5 4 1]	57	-2.261	11/2	11/2 [6 1 5]
14	-21.292	-5/2	5/2 [3 1 2]	36	-10.280	-7/2	7/2 [5 2 3]	58	-2.207	-1/2	1/2 [7 5 0]
15	-20.333	-7/2	7/2 [3 0 3]	37	-9.794	1/2	1/2 [4 1 1]	59	-2.182	7/2	7/2 [5 0 3]
16	-19.621	-3/2	3/2 [3 1 2]	38	-9.301	5/2	5/2 [4 0 2]	60	-1.773	3/2	3/2 [6 4 2]
17	-19.254	1/2	1/2 [4 2 0]	39	-9.054	-9/2	9/2 [5 1 4]	61	-1.669	1/2	1/2 [6 4 0]
18	-18.229	-5/2	5/2 [3 0 3]	40	-8.356	-3/2	3/2 [5 3 2]	62	-1.553	-3/2	3/2 [7 4 1]
19	-18.189	3/2	3/2 [4 3 1]	41	-8.276	1/2	1/2 [6 4 0]	63	-1.459	13/2	13/2 [6 0 6]
20	-18.130	-1/2	1/2 [3 1 0]	42	-8.217	-11/2	11/2 [5 0 5]	64	-1.118	-3/2	3/2 [5 1 2]
21	-16.730	5/2	5/2 [4 2 2]	43	-7.624	-1/2	1/2 [5 3 0]	65	-1.065	-1/2	1/2 [5 1 0]
22	-16.416	1/2	1/2 [4 3 1]	44	-7.597	3/2	3/2 [6 5 1]	66	-0.393	-5/2	5/2 [7 5 2]

creation of new many particle-hole configurations in competition with particles emission and fission, and for some doorway configurations it might have nonstatistical character, but, as a first guideline for order of magnitude estimates we calculate the total fission probability (nucleus with energy E^* deexcites in several steps) on the statistical theory grounds, both with and without taking into account the preequilibrium decay.

A. Compound nucleus model

First, we considered an extreme situation, by assuming that the residual interaction leads to thermalization and formation of compound nucleus just after the fast reaction stage, without any preequilibrium particle emission. In this case, the compound nucleus excitation energy is assumed to be

$$E^* = -E_\alpha + \varepsilon_f, \quad (31)$$

where E_α is the energy of the bound state (hole).

For calculations of compound nucleus fissionity we used the Bohr-Wheeler [12] and Weisskopf [13] models for the description of the evaporation/fission competition. We developed a Monte Carlo algorithm for the evaporation/fission processes, which includes not only the neutron evaporation vs fission competition, but also takes into account the proton and α -particle contributions.

The probability for the emission of a particle j with kinetic energy between E_k and $E_k + dE_k$ is calculated within the Weisskopf statistical model [13] as

$$P_f(E_k)dE_k = \gamma_j \sigma_j E_k \left(\frac{\rho_f}{\rho_i} \right) dE_k, \quad (32)$$

where σ_j is the nuclear capture cross section for the particle j , $\gamma_j = gm/\pi^2 h^3$, where g denotes the number of spin states and m is the particle mass. The level densities for the initial

and final nucleus, ρ_i and ρ_f , respectively, are calculated from the Fermi gas expression

$$\rho(E_j^*) = \exp[2(aE_j^*)^{1/2}],$$

where a is the level density parameter (see below),

$$E_j^* = E^* - (B_j + V_j), \quad (33)$$

where E^* is the nuclear excitation energy in the initial state, B_j is the particle separation energy, and V_j is the Coulomb barrier corrected for the nuclear temperature τ defined by $E^* = a\tau^2$.

The particle emission width is calculated as

$$\Gamma_j = \int_0^{E_j^*} P_j(E_k) dE_k. \quad (34)$$

From this general equation, the k -particle emission probability relative to the j -particle emission is

$$\frac{\Gamma_k}{\Gamma_j} = \left(\frac{\gamma_k E_k^* a_j}{\gamma_j E_j^* a_k} \right) \exp[2\{(a_k E_k^*)^{1/2} - (a_j E_j^*)^{1/2}\}]. \quad (35)$$

The level density parameter for neutron emission is [14]

$$a_n = (0.134A - 1.21 \times 10^{-4} A^2) \text{ MeV}^{-1}, \quad (36)$$

and for all other particle emission this quantity is related to a_n by

$$a_j = r_j a_n, \quad (37)$$

where r_j is an adimensional constant.

Shell model corrections [15] are not taken into account. For high excitation energies their effects are likely to cancel each other upon averaging over all possible nuclei created during the reaction.

Using the fission width from the liquid drop model [12], and the neutron emission width from Weisskopf [13], we get

$$\frac{\Gamma_f}{\Gamma_n} = K_f \exp[2\{(a_f E_f^*)^{1/2} - (a_n E_n^*)^{1/2}\}], \quad (38)$$

where

$$K_f = K_0 a_n \frac{2(a_f E_f^*)^{1/2} - 1}{4A^{2/3} a_f E_n^*} \quad (39)$$

with $K_0 = 14.39 \text{ MeV}$ and $E_j^* = E^* - B_f$. Here B_f is the fission barrier height discussed below.

For proton emission we get

$$\frac{\Gamma_p}{\Gamma_n} = \left(\frac{E_p^*}{E_n^*} \right) \exp[2(a_n)^{1/2}\{(r_p E_p^*)^{1/2} - (E_n^*)^{1/2}\}], \quad (40)$$

and for α -particle emission [14,16]

$$\frac{\Gamma_\alpha}{\Gamma_n} = \left(\frac{2E_\alpha^*}{E_n^*} \right) \exp[2(a_n)^{1/2}\{(r_\alpha E_\alpha^*)^{1/2} - (E_n^*)^{1/2}\}]. \quad (41)$$

In the above equations, the Coulomb potential for protons is [17]

$$V_p = C \frac{k_p(Z-1)e^2}{r_0(A-4)^{1/3} + R_p}, \quad (42)$$

and for α particles,

$$V_\alpha = C \frac{2K_\alpha(Z-2)e^2}{r_0(A-4)^{1/3} + R_\alpha}, \quad (43)$$

where $K_p = 0.70$ and $K_\alpha = 0.83$ are the Coulomb barrier penetrability for protons and α particles, respectively; $R_p = 1.14 \text{ fm}$ is the proton radius; $R_\alpha = 2.16 \text{ fm}$ is the α particle radius; and $r_0 = 1.2 \text{ fm}$. The factor C introduces in a semiempirical way the dynamical effects in particle separation energy and fission barrier due to the nuclear temperature [17], namely,

$$C = 1 - \frac{E^*}{B}, \quad (44)$$

where B is the total nuclear binding energy ($B = 1794 \text{ MeV}$ for ^{237}Pa [17]).

The fission barrier is calculated by [17]

$$B_f = C(0.22[A-Z] - 1.40Z + 101.5) \text{ MeV}. \quad (45)$$

The neutron separation energy was taken as 5.78 MeV for the first step (^{237}Pa), and for the other steps as [15]

$$B_n = (-0.16(A-Z) + 0.25Z + 5.6) \quad (46)$$

while the proton and α -particle separation energies are calculated through the nuclear mass formula [18]

$$B_p = m_p + M(A-1, Z-1) - M(A, Z), \quad (47)$$

where m_p is the proton mass and $M(A, Z)$ is the nuclear mass calculated with the parameters from Ref. [18]. For the α particles we get

$$B_\alpha = m_\alpha + M(A-4, Z-2) - M(A, Z), \quad (48)$$

where m_α is the α particle mass.

These values reproduce the experimental data for P_f (see discussion below).

The present Monte Carlo code for evaporation fission calculates, at each step i of the evaporation chain, the fission probability F_i defined as

$$F_i = \frac{\left(\frac{\Gamma_f}{\Gamma_n} \right)_i}{1 + \left(\frac{\Gamma_f}{\Gamma_n} \right)_i + \left(\frac{\Gamma_p}{\Gamma_n} \right)_i + \left(\frac{\Gamma_\alpha}{\Gamma_n} \right)_i}.$$

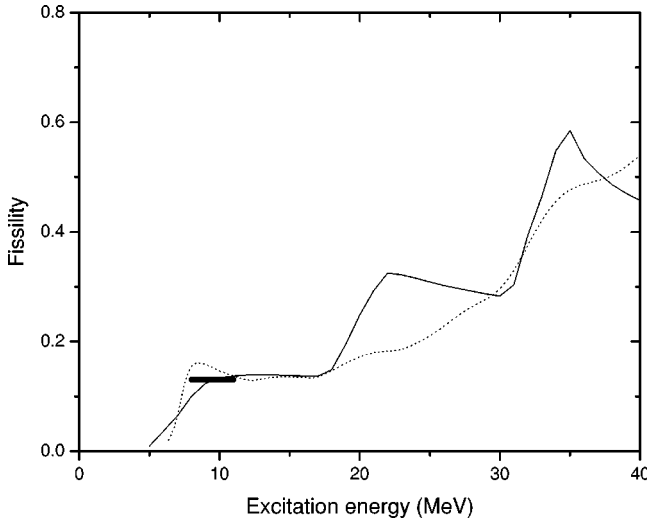


FIG. 3. Fissionity of ^{237}Pa vs the hole excitation energy. The solid curve shows the compound nucleus model calculation, assuming that the hole excitation energies correspond to the compound nucleus excitation energies: the complete thermalization is reached without any preequilibrium decay. The dotted curve corresponds to the exciton model calculations, that take into account the preequilibrium decay. The rectangle shows the extrapolated experimental data (see text for details).

An evaporating particle j is randomly chosen (neutron, proton, or α particle), according to its relative branching ratios. Once one of these particles is chosen, the mass and atomic numbers are recalculated through

$$A_{i+1} = A_i - \Delta A_i,$$

and

$$Z_{i+1} = Z_i - \Delta Z_i,$$

where ΔA_i and ΔZ_i are, respectively, the mass and atomic numbers of the ejected particle at the i th step in the evaporation process. The nuclear excitation energy is modified according to the expression

$$E_{i+1}^* = E_i^* - B_i - T_i,$$

where B_i and T_i are the separation and the asymptotic kinetic energies of the particle being ejected, respectively. For neutrons $T=2$ MeV, and for protons and α particles $T=0$ MeV. The expressions described above ensure that the nuclear excitation energy will be, at each step in the evaporation chain, smaller than in the previous step. This process continues until the excitation energy available in the nucleus is not enough to emit any one of the possible evaporating particles. At this point the evaporation process stops, and we can calculate the nuclear fissionity by the expression

$$W = \sum_i \left[\prod_{j=0}^{i-1} (1 - F_j) \right] F_i. \quad (49)$$

Using the model described above, we calculated the fissionity for ^{237}Pa (Fig. 3, solid curve). Peaks observed for the

fissionity reflect the opening of the fission channel in the daughter nuclei. Figure 3 also shows (rectangle) the data for the fissionity of ^{237}Pa obtained by extrapolation of the neutron to fission widths ratios for $Z=91$, and $A=230-237$ [19], by using the empirical trend presented in Vandenbosch and Huizenga [16].

It should be pointed out that in our calculations of the fissionity we assumed that the hole excitation energies for an $A-1$ nucleus correspond to the compound nucleus excitation energies, that is to say, the complete thermalization is reached without any preequilibrium decay. Such calculations could be considered as an upper limit estimate for the fissionity.

B. Exciton model

During the thermalization of the hole excitation energy, the nucleus $A-1$ could undergo particle evaporation (preequilibrium decay [20,21]).

In this case, the energy of the hole is not attributed to the nuclear temperature but, instead, assumed as a characteristic of the doorway state in the thermalization process followed by the emission of particles or fission.

The calculation involving the preequilibrium decay was performed within the framework of the exciton model [22], using the code STAPRE. In this model, the states of the system are classified according to the number of excitons n , which corresponds to the total number of excited particle p and hole h degrees of freedom, $n=p+h$. The exciton model included in STAPRE does not distinguish between protons and neutrons. Starting from a simple configuration of low exciton number, the system is assumed to equilibrate through a series of two-body collisions and to emit particles from all intermediate states. The application of a two-body interaction to the states of a (p, h) configuration results in states with $(p+1, h+1)$, (p, h) , and $(p-1, h-1)$ excited particles and holes. The difference between the number of excited particles and holes remains fixed, justifying the use of the exciton number to label the states. However, the transition rates, which are an average over all states of a configuration, do depend on the number of excited particles and holes. The equation governing the time development of the occupation $P(n)$ of the n th exciton configuration can thus be written as

$$\begin{aligned} \frac{dP(n)}{dt} = & \lambda_-(n+2)P(n+2) + \lambda_0(n)P(n) \\ & + \lambda_+(n-2)P(n-2) - \lambda(n)P(n), \end{aligned} \quad (50)$$

where $\lambda(n)$ is the total transition rate

$$\lambda(n) = \lambda_-(n) + \lambda_0(n) + \lambda_+(n) + \lambda_e(n) \quad (51)$$

with $\lambda_e(n)$ being the total rate of particle emission from the n th exciton configuration. The quantities $\lambda_-(n)$, $\lambda_0(n)$, and $\lambda_+(n)$ are the average rates for internal transitions from the n th exciton configuration with a change of exciton numbers by -2 , 0 , or $+2$.

The internal transition rates can be written as the product of the average squared matrix element of the residual inter-

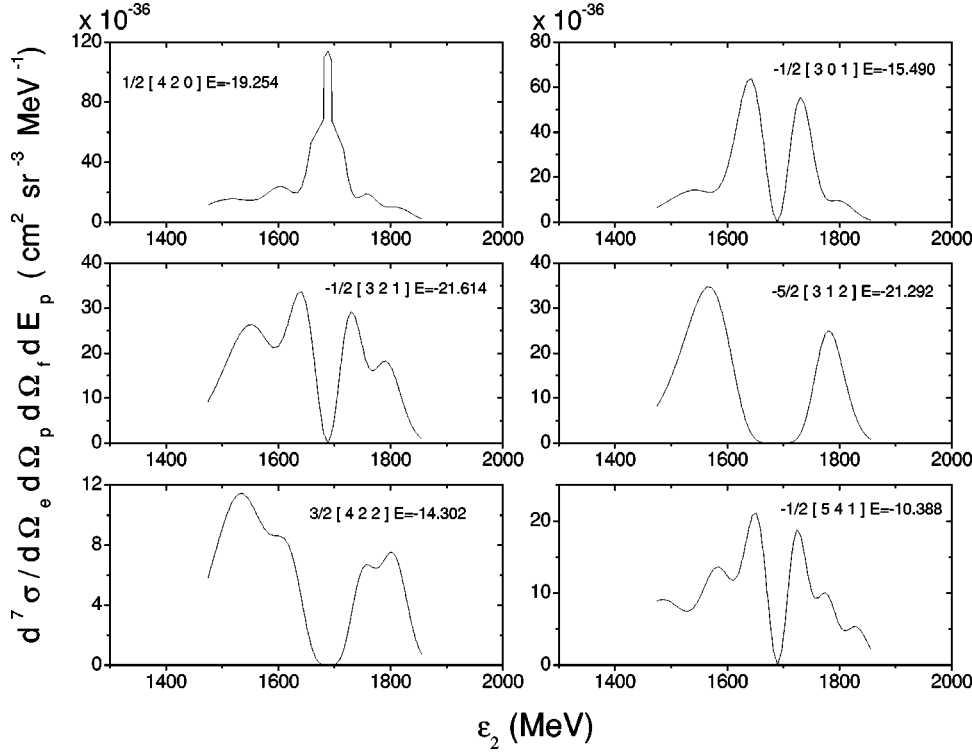


FIG. 4. Sevenfolded differential cross sections for the parallel kinematics. The calculations of the cross sections were accomplished for $\varepsilon_1 = 2000$ MeV, $\theta_e = 23^\circ$, $\phi = 0^\circ$. The cross section for $E = -10.388$ MeV state (sub-barrier) is multiplied by 100.

action $|M|^2$ with the relative density of available states. For the latter, STAPRE uses the expressions of Williams [23] as corrected for the Pauli principle by Cline [24]. These yield

$$\lambda_-(n) \equiv \lambda_-(p, h, E) = \frac{2\pi}{\hbar} |M|^2 \frac{g(gE - C_{p+1, h+1})^2}{p+h+1},$$

$$\lambda_0(n) \equiv \lambda_0(p, h, E) = \frac{2\pi}{\hbar} |M|^2 g(p+h-1)(gE - C_{p, h}),$$

$$\lambda_+(n) \equiv \lambda_+(p, h, E) = \frac{2\pi}{\hbar} |M|^2 g p h (p+h-2), \quad (52)$$

where

$$C_{p, h} = \frac{1}{2}(p^2 + h^2)$$

with E the excitation energy of the system. The parameter g is the single-particle state density, which is taken to be $g = (6/\pi^2)a$, with a as the level density parameter. Following Ref. [25], the average matrix element is approximated as

$$|M|^2 = \frac{f_M}{A^3 E},$$

where A is the mass number of the system and f_M is a parameter, which we assumed to be $f_M = 230$ MeV³ in our calculations.

The particle emission rate $\lambda_e(n)$ is the sum of the integrated proton and neutron differential emission rates $\lambda_{e\nu}(n, \varepsilon) d\varepsilon_\nu$, which are determined through considerations of detailed balance [24],

$$\begin{aligned} \lambda_{e\nu}(n, \varepsilon) d\varepsilon_\nu &\equiv \lambda_{e\nu}(p, h, E, \varepsilon_\nu) d\varepsilon_\nu \\ &= \frac{1}{\pi^2 \hbar^3} \mu_\nu \varepsilon_\nu \sigma_\nu(\varepsilon_\nu) R_\nu \\ &\quad \times \frac{\omega(p-1, h, E - B_\nu - \varepsilon_\nu)}{\omega(p, h, E)} d\varepsilon_\nu, \quad (53) \end{aligned}$$

where μ_ν is the reduced mass of the emitted neutron/proton, ε_ν is its outgoing kinetic energy, B_ν is its separation energy, and $\sigma_\nu(\varepsilon_\nu)$ is the cross section for the inverse absorption process. The factor R_ν is a simple correction standing for the fact that neutrons and protons have not been distinguished in the process; thus,

$$R_\nu = \begin{cases} N/A & \text{for neutron emission} \\ Z/A & \text{for proton emission.} \end{cases}$$

The densities of states are taken to be the Williams densities

$$\omega(p, h, E) = \frac{g(gE - A_{p, h})^{p+h-1}}{p! h! (p+h-1)!}, \quad (54)$$

where the Pauli blocking correction is

$$A_{p, h} = \frac{1}{4}(p^2 + h^2 + p - 3h).$$

The differential emission rates differ from those of usual Weisskopf compound nucleus emission by the factor R_ν and by the use of exciton state densities rather than compound nucleus ones.

The time evolution equation, Eq. (50), forms a set of coupled linear differential equations whose solution could be written in the form of a vector as

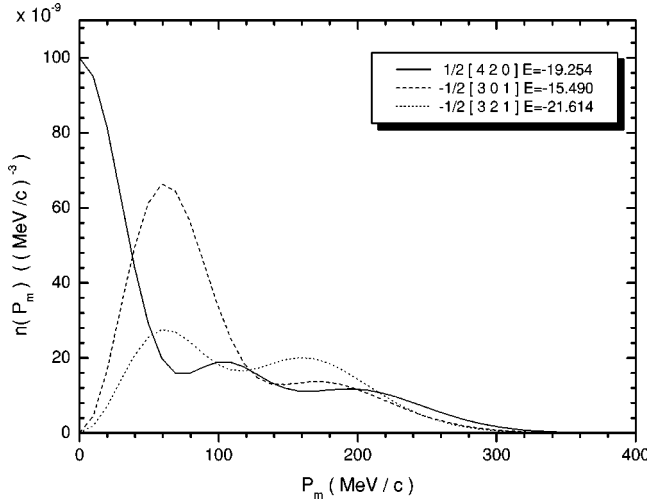


FIG. 5. Momentum distributions for some proton bound states having maxima at the low missing momentum region.

$$\vec{P}(t) = \exp[-\Lambda t] \vec{P}_0,$$

where the matrix Λ is given by

$$\Lambda_{nn'} = \lambda(n) \delta_{n',n} - \lambda_-(n+2) \delta_{n',n+2} - \lambda_0(n) \delta_{n',n} - \lambda_+(n-2) \delta_{n',n-2},$$

and the vector \vec{P}_0 describes the initial exciton configuration of the system,

$$P_0(n) \equiv P_0(p, h) = \delta_{p,p_0} \delta_{h,h_0}.$$

The decay of the system into all possible final configurations can be obtained by integrating the total emission rate over all time,

$$\sum_n \int_0^\infty \lambda_e(n) P(n, t) dt = \sum_{n,n'} \lambda_e(n) (\Lambda^{-1})_{n,n'} P_0(n'). \quad (55)$$

The decay of the fraction of the initial probability, which survives preequilibrium emission, is described using the Hauser-Feshbach formalism. We have considered fission in competition with neutron and gamma emission.

The initial configuration in ^{237}Pa consists of one particle at the Fermi level and one hole in a bound state. This configuration is consistent with the proton knock-out reaction for ^{238}U initiating the statistical cascade. Our calculations were performed assuming a one-hole initial configuration of the $l=0$ partial wave alone. The particle at the Fermi level contributes negligibly to the equilibration process. The fission barriers, neutron separation energies, and level density parameters were taken to be the same as those of the compound nucleus calculations in the preceding section.

The exciton model fissility results for single-hole states of ^{237}Pa are shown in Fig. 3 by the dotted curve. We note that these calculations for fissility show a smoother behavior than that for compound model. The preequilibrium particle emis-

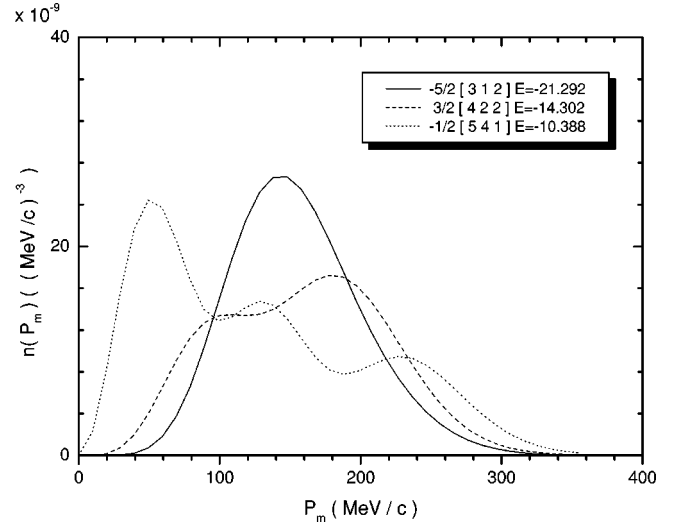


FIG. 6. Momentum distributions for some proton bound states having maxima at the high missing momentum region.

sion removes some excitation energy before an equilibrium is reached reducing, therefore, the probability of opening new chances for fission.

V. FINAL RESULTS

The differential cross section for the $(e, e' pf)$ reaction was obtained by assuming an isotropic angular distribution for the fission fragments, and the fissility as a factor,

$$\frac{d^7 \sigma}{d\Omega_e d\Omega_p dE_p d\Omega_f} = \frac{1}{4\pi} \frac{d^5 \sigma}{d\Omega_e d\Omega_p dE_p} P_f \quad (56)$$

Figure 4 shows the sevenfold differential cross sections $d^7 \sigma / d\Omega_e d\Omega_p dE_p d\Omega_f$ for some bound proton states (Table I) and the compound nucleus model fissility (solid curve in Fig. 3) calculated for $\varepsilon_1 = 2000$ MeV, $\theta_e = 23^\circ$ and the parallel kinematics [26]. In this kinematics ε_1 and θ_e are fixed,

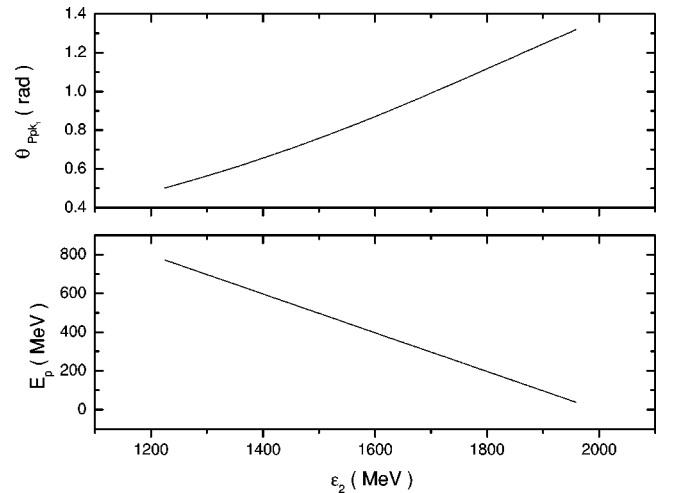


FIG. 7. Variation of the angle θ_{p,k_1} (see Fig. 1) and the outgoing proton kinetic energy E_p vs ε_2 for the parallel kinematics and $\varepsilon_1 = 2000$ MeV, $\theta_e = 23^\circ$.

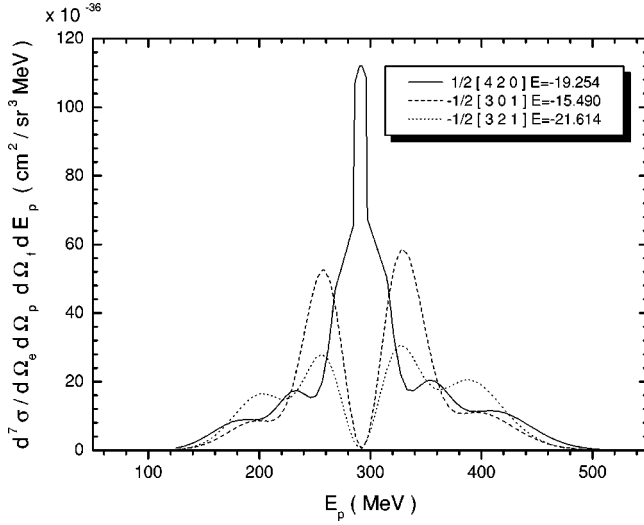


FIG. 8. Differential cross sections for some bound states of ^{238}U , having maxima of the momentum distributions at the low missing momentum region. The calculations of the cross sections were accomplished for $\varepsilon_1=2000$ MeV, $\theta_e=23^\circ$, $\phi=0^\circ$, and $\theta_{p_p k_1}=0.98$ rad.

and for each value of ε_2 the proton spectrum is measured in the direction of \vec{q} , varying each time the angle $\theta_{p_p k_1}$ (see Fig. 1). For such scheme of measurements the initial (missing) momentum of the proton \vec{p}_m is always parallel (or antiparallel) to \vec{q} . The parallel kinematics simplify the accounting of FSI, since there are no contribution of interference terms in the cross sections [see Eqs. (9)]. Figures 5 and 6 show the momentum distributions for states used in the calculation of the cross sections presented in Fig. 4, and Fig. 7 shows the outgoing proton kinetic energy and angle $\theta_{p_p k_1}$ vs ε_2 for the parallel kinematics we use.

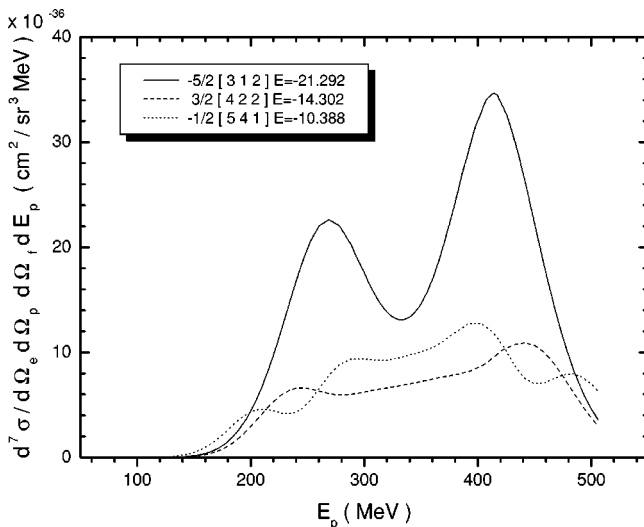


FIG. 9. The same as in Fig. 8, but for some bound states of ^{238}U , having maxima of the momentum distributions at the high missing momentum region and for $\theta_{p_p k_1}=0.82$ rad.

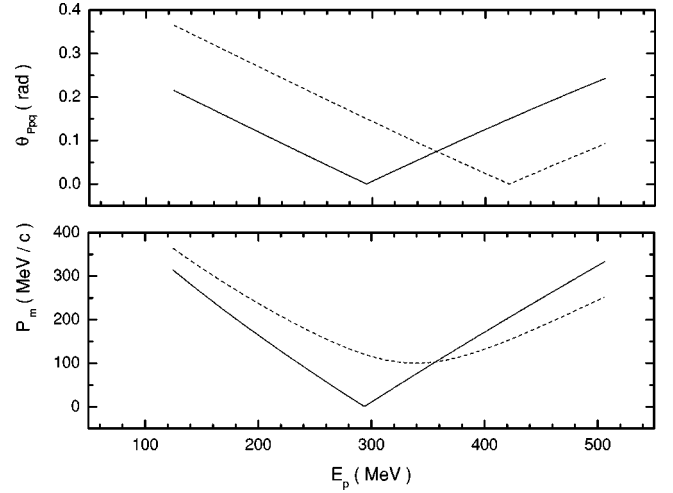


FIG. 10. Missing momentum P_m and angle $\theta_{p_p q}$ as functions of the outgoing proton kinetic energy for $\theta_{p_p k_1}=0.98$ rad (solid curve) and 0.83 rad (dashed curve).

Figures 8 and 9 show the differential ($e, e' p f$) cross sections calculated for the same ε_1 and θ_e but for two fixed proton angles: $\theta_{p_p k_1}=0.98$ rad for the group of proton states of ^{238}U , which have a maximum in the low missing momentum region (Fig. 5), and $\theta_{p_p k_1}=0.82$ rad for the group having a maximum in the high missing momentum region (Fig. 6). These angles $\theta_{p_p k_1}$ were chosen in order to achieve parallel kinematics, that is $\theta_{p_p q} \approx 0$, and maximum for cross sections at both the low ($\theta_p=0.98$ rad) and high ($\theta_p=0.82$ rad) missing momentum regions. Figure 10 shows the missing momentum P_m and the angle $\theta_{p_p q}$ as functions of the outgoing proton kinetic energy for $\theta_p=0.98$ rad (solid curve) and 0.83 rad (dashed curve).

It is seen from the Figs. 8, 9, and 10 that for such a choice the cross sections have maxima at E_p around 300 and 400 MeV and, for these energies, the proton angles $\theta_{p_p q}$ are small (parallel kinematics).

The differential cross sections presented in Figs. 4, 8, and 9 correspond to the situation when the hole excitation energies for an $A-1$ nucleus are the compound nucleus excitation energies, that is to say, the complete thermalization is reached without any preequilibrium decay. Such calculations could be considered as an upper limit estimate for the cross section.

VI. CONCLUSIONS

We presented a theoretical study for the quasifree electrofission of ^{238}U . The proton bound states were calculated in the framework of the macroscopic-microscopic approach, using the axially deformed Woods-Saxon single-particle potential. The occupation numbers were calculated in the BCS approach.

The exclusive differential cross sections for the quasifree scattering reaction stage were calculated in PWIA using off-shell electron-nucleon cross sections.

The fissility for the single-hole states of the residual nucleus ^{237}Pa was calculated in the framework of two approaches: compound nucleus model without taking into account the preequilibrium emission of the particles, and the exciton model accounting for preequilibrium emission. Both models exhibit the same general trend, but the fissility as given by the preequilibrium model is smoother.

The obtained results could serve as a first guideline on

order of magnitude estimates of the expected cross sections for quasifree electrofission of ^{238}U .

ACKNOWLEDGMENTS

The authors thank the Brazilian agencies CNPq and FAPESP for the partial support to this work and the graduate students W. R. Carvalho, M. S. Vaudeluci, and L. F. R. Macedo for their help.

-
- [1] L.S. Cardman, Nucl. Phys. **A654**, 73 (1999).
 - [2] V. P. Likhachev *et al.*, Phys. Rev. C (to be submitted).
 - [3] K. Hansen *et al.*, Phys. Rev. C **41**, 1619 (1990).
 - [4] T. de Forest, Nucl. Phys. **A392**, 232 (1983).
 - [5] F. Garcia, O. Rodriguez, J. Mesa, J.D.T. Arruda-Neto, V.P. Likhachev, E. Garrote, R. Capote, and F. Guzmán, Comput. Phys. Commun. **120**, 57 (1999).
 - [6] V.V. Pashkevich, Nucl. Phys. **A169**, 275 (1971).
 - [7] F.A. Ivanyuk, H. Hofmann, V.V. Pashkevich, and S. Yamaji, Phys. Rev. C **55**, 1730 (1997).
 - [8] F. Garcia, E. Garrote, M.-L. Yoneama, J.D.T. Arruda-Neto, J. Mesa, F. Bringas, J.F. Dias, V.P. Likhachev, O. Rodriguez, and F. Guzmán, Eur. Phys. J. A **6**, 49 (1999).
 - [9] V.A. Chepurnov, Sov. J. Nucl. Phys. **6**, 696 (1968).
 - [10] F. Garcia, O. Rodriguez, V.A. Rubchenya, and E. Garrote, Comput. Phys. Commun. **86**, 129 (1995).
 - [11] F. Garcia, O. Rodriguez, E. Garrote, and E. Lopez, J. Phys. G **19**, 2157 (1993).
 - [12] N. Bohr and J.A. Wheeler, Phys. Rev. **56**, 426 (1939).
 - [13] V. Weisskopf, Phys. Verh. **72**, 1114 (1947).
 - [14] A.S. Iljinov *et al.*, Nucl. Phys. **B32**, 166 (1980).
 - [15] C. Guaraldo *et al.*, Il Nuovo Cim. **103**, 607 (1990).
 - [16] R. Vandenbosch and J. R. Huizenga, *Nuclear Fission*, 1st ed. (Academic, New York, 1973), p. 227.
 - [17] O.A.P. Tavares and M.L. Terranova, Z. Phys. A: Hadrons Nucl. **343**, 407 (1992).
 - [18] E. Segrè, *Nuclei and Particles: An Introduction to Nuclei and Subnuclei Physics*, 3rd ed. (Benjamin, New York, 1965).
 - [19] A. Gavron *et al.*, Phys. Rev. C **13**, 2374 (1976).
 - [20] R. Bonetti, M.B. Chadwick, P.E. Hodgson, B.V. Carlson, and M.S. Hussein, Phys. Rep. **202**, 171 (1991).
 - [21] E. Gadioli and P. E. Hodgson, *Pre-equilibrium Nuclear Reactions* (Oxford University Press, Oxford, 1992).
 - [22] C. Kalbach, Acta Phys. Slov. **25**, 100 (1975).
 - [23] F.C. Williams, Jr., Phys. Lett. **31B**, 184 (1970).
 - [24] C.K. Cline, Nucl. Phys. **A186**, 273 (1972).
 - [25] C. Kalbach-Cline, Nucl. Phys. **A210**, 590 (1973).
 - [26] J. Potter, Nucl. Phys. **45**, 33 (1963).